Structural relaxation in the dynamics of glycerol: a joint visible, UV and x-ray inelastic scattering study

2006 J. Phys.: Condens. Matter 18 889

(http://iopscience.iop.org/0953-8984/18/3/008)

INSTITUTE OF PHYSICS PUBLISHING JOURNAL OF PHYSICS: CONDENSED MATTER

J. Phys.: Condens. Matter **18** (2006) 889–902 doi:10.1088/0953-8984/18/3/008

Structural relaxation in the dynamics of glycerol: a joint visible, UV and x-ray inelastic scattering study

A Giugni[1,2] **and A Cunsolo**[3]

[1] INFM UdR L'Aquila, and Universitá dell'Aquila L'Aquila, Italy
[2] INFM CRS-SOFT, c/o Universitá di Roma 'La Sapienza', I-00185, Roma, Italy
[3] INFM-OGG and CRS SOFT c/o Institut Laue Langevin 6 rue, J. Horowitz, BP156 38042 Grenoble Cedex 9, France

Received 29 July 2005, in final form 5 December 2005
Published 6 January 2006
Online at stacks.iop.org/JPhysCM/18/889

Abstract

We describe an experimental study of the dynamic structure factor of liquid glycerol performed by complementary inelastic techniques such as Brillouin visible, ultraviolet and x-ray scattering. The spectra have been collected as a function of both temperature and momentum transfer. The relevant hypersonic parameters are evaluated from the spectral lineshape analysis modelling the data with a simple hydrodynamic profile. The study of their frequency dependence allows us to observe the occurrence of an active structural relaxation and to measure the related timescale. We also find signatures of further relaxation processes occurring below the accessible frequency window. As a result, the dynamic window traditionally probed in spectroscopic experiments is greatly extended and partially bridges the gap between MHz and THz techniques.

1. Introduction

The breakdown of hydrodynamic behaviour in liquid systems has been the focus of a host of experimental [1–6], computational [7] and theoretical works [8]. In spite of all these thorough studies an exhaustive understanding of all the microscopic processes responsible for such crossover still remains one of the main challenges of condensed matter physics [8].

To get a physical insight into this subject we can start from considering that in a liquid the propagation of a spontaneous or excited density wave perturbs the local structure of the neighbouring medium. As a response, new local equilibria are then restored by means of energy transfer from sound waves towards some internal degree of freedom. These rearrangements are usually referred to as relaxation processes. If their timescale, τ, is much shorter than the period of the acoustic waves, the latter propagates adiabatically, i.e. over successive local equilibrium states. This is the so-called hydrodynamic or *viscous regime* that characterizes the low-frequency acoustic propagation in simple fluids. In the opposite *elastic regime* sound waves with a period much shorter than τ are probed. Under such conditions, the fluid's internal rearrangements are too slow to dissipate the energy carried by the acoustic excitation, which therefore propagates almost elastically, i.e. without losing energy. In the intermediate

viscoelastic regime the probed sound wave has a period comparable with τ and, therefore, it turns out to be strongly coupled with the relaxation mechanisms active in the fluid [8].

The occurrence of a relaxation phenomenon has a characteristic effect on the q dispersion of the acoustic excitations, mainly consisting in a bending of q-dispersion curve upwards with respect to the linear hydrodynamic prediction (*positive sound dispersion*).

It is customary to distinguish between different relaxation processes according to the specific degree of freedom involved in the energy redistribution. Among them, structural relaxations are of major interest in the physics of glass formers since they involve cooperative readjustments of local structure responsible, for example, for formation of the glass [9]. These processes are characterized by a timescale τ_α having a sharp temperature dependence roughly paralleling that of the viscosity [1]. In the literature these processes have been characterized over 14 orders of magnitude in the time or frequency domain [10] and in a host of disordered systems [2, 1, 14, 13, 15].

On the experimental side, hints on structural relaxations can in principle be obtained by looking at the evolution of the dynamic structure factor $S(q, \omega)$ with the exchanged momentum, q, and temperature, T, between viscous and the elastic regimes.

Glass forming systems seem best suited to this purpose, mainly owing to the strong T dependence of τ_α which allows the viscoelastic window, defined as $\omega \approx 2\pi/\tau_\alpha$, to be brought inside any desired frequency range. In the past, the study of relaxation processes in glass formers has been pursued by looking at the evolution with T of $S(q, \omega)$ at nearly constant q [2]. However, this method suffers from a major 'intrinsic' limitation since the dynamic behaviour of the fluid is studied by comparing disparate thermodynamic states, i.e. imposing different physical constraints on the sample. On rigorous grounds, T should be fixed while changing q; unfortunately this method suffers from important difficulties. In fact, as far as the lower portion of the kinematic plane is involved, Brillouin light scattering (BLS) seems rather unsuitable for spanning a wide range of q. Moreover the occurrence, at low q, of rather complex multiple timescale relaxations often makes the lineshape analysis quite delicate and slightly dependent on the adopted model [2, 4]. On the other hand, other available high-frequency techniques, such as inelastic x-ray or neutron scattering (IXS and INS respectively), cover a time domain shorter by more than a decade than the one typical of structural relaxation of liquid glass formers. Finally, an accurate best fit analysis of IXS or INS spectra is often prevented by limited instrumental resolution.

All these difficulties strongly suggest the simultaneous use of complementary spectroscopic techniques. Nowadays this result could be achieved thanks to the recent development of a novel high-resolution intermediate q inelastic technique: Brillouin ultraviolet scattering (BUVS) [16]. Being aware of this opportunity, we decided to study the evolution of $S(q, \omega)$ with q and T for liquid glycerol in its normal liquid phase, simultaneously employing BLS, BUVS and IXS. Specifically, BLS and BUVS were employed to cover the 5.6×10^{-3} nm$^{-1} \leqslant q \leqslant 0.71 \times 10^{-1}$ nm^{-1} q range (1.6 GHz $\leqslant \omega/2\pi \leqslant$ 33 GHz) while IXS was used to probe the $q = 2$ and 4 nm^{-1} ($\nu = \omega/2\pi \approx$ 800–900 GHz).

Within Angell's classification scheme [11] glycerol, $T_m = 291$ K, $T_g = 185$ K, belongs to the class of glass formers of intermediate fragility, and it seems a natural candidate for such a study. Though structural relaxations in this system have already been characterized over a broad frequency and temperature range by a variety of spectroscopic techniques [2, 1, 13–15], as well as by calorimetric [17] and dielectric measurements [18], the various results reported exhibit some inconsistencies when the system approaches its glass transition [10, 15].

The experimental spectra of glycerol have been customarily described within the so-called Mori–Zwanzig formalism [12], where the time decay of the memory function is retrieved by a distribution of the form $\exp(t/\tau_\alpha)^\beta$. It has been found that, in the supercooled regime, the

stretching parameter β slightly decreases with T, consistent with what has been observed in other intermediate or fragile glass formers.

In this experiment the lineshape analysis of glycerol spectra was performed using a simple hydrodynamic model, which allows a direct evaluation of both apparent sound velocity and longitudinal kinematic viscosity. We show that the frequency dependence of these parameters mainly has the form of a Cole–Davidson (CD) profile. The values of the characteristic relaxation time, $\tau_0(T)$, and the stretching parameter, $\beta(T)$, have been evaluated requiring the CD profiles to fit the sound velocity and the viscosity data. As result, the low-frequency side of the best fit CD distributions appear, at least for the sound velocity parameter, to be fairly consistent with the literature ultrasound (US) measurements [13], despite the different (MHz) dynamic region involved.

Nevertheless, best fit CD profiles for longitudinal kinematic viscosity suggest, to overcome the experimental mismatch with US results, the occurrence of an additional frequency relaxation below the frequency window accessed in our experiment. Finally we observe that our data fully agree with previous BLS measurements probing an overlapping, yet narrower, dynamic region [2].

2. The experiment

2.1. BLS and BUVS measurements

The experimental assembly consists of a high-resolution high-contrast Brillouin spectrometer recently set up at the University of L'Aquila, whose performance and working principles have been described in detail elsewhere [16]. The instrument comprises a home-made double-grating 4 m focal length assembly *ad hoc* designed for Brillouin spectroscopy, tunable to select either visible ($\lambda = 532$ nm) or ultraviolet ($\lambda = 266$ nm) excitation lines. The two monochromators are mounted in a modified Fastie–Ebert additive configuration working under strict Littrow conditions. Echelle gratings (31.6 grooves mm^{-1}) were used, blazed to work at $N = 115$ and diffraction order 230 for the wavelength sources $\lambda = 532$ and 266 nm, respectively. The measured diffraction-limited full-width half-maximum (FWHM) resolution is 330 MHz at 532 nm and 450 MHz at 266 nm. The lineshape properties of the double monochromator response function yield a measured contrast of the order of 10^{10} at $\sim$30 GHz.

The visible linearly polarized source is provided by a compact solid-state diode-pumped frequency-doubled Nd:YVO_4 laser (Coherent Inc., model Verdi) delivering a single-mode beam having 5 W power at 532 nm; UV radiation is generated through a second frequency duplication via a nonlinear BBO single crystal in the near UV ($\lambda = 266$ nm). The scattering angle can be varied continuously from a few degrees, close to forward scattering geometry, up to back-scattering geometry, by rotating a platform bearing the laser source itself. The monochromator stage is kept entirely under a temperature-controlled helium atmosphere which reduces the effects of local density fluctuations along the rather long beam path ($\simeq$40 m from entrance to exit slits), and improves the overall thermal stabilization of the instrument. The frequency scan is achieved by simultaneous rotation of the two gratings. The scattered intensity is collected by a low-noise photomultiplier tube working in single-photon counting mode.

In the present experiment the laser beam with wavelength 532 nm ($\simeq$2 W power) was focused into the sample by means of a 250 mm focal length lens and lower power level and unfocused conditions were, instead, used at 266 nm ($\leqslant$200 mW) to reduce sample heating originating from increased sample absorption in the ultraviolet.

Spectra were typically collected in frequency steps of 50–100 MHz at 532 nm (200 MHz at 266 nm) with a resolution of about 400–500 MHz (700–800 MHz) as measured from the

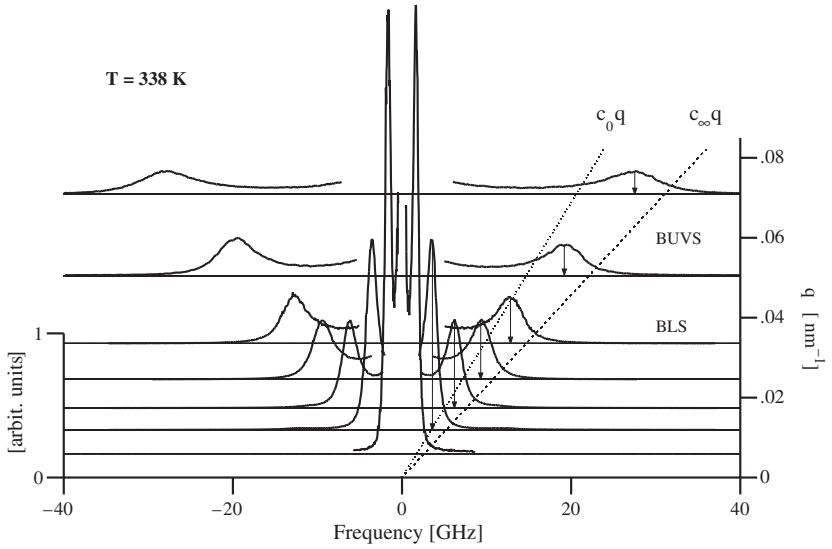

Figure 1. Typical Brillouin spectra of glycerol obtained with visible (532 nm) and ultraviolet (266 nm) incident radiation, collected in V–U back-scattering geometry at $T = 338$ K. The intensity is normalized to the second spectral moment. Low-frequency (viscous) and high-frequency (elastic) linear sound dispersions are also reported for comparison (dotted lines). Vertical arrows show the inelastic peak position.

FWHM of the spectral density of a fused silica sample which behaves as an almost elastic scatterer. The scattering angles, ϑ, ranging from 20° to 180° were measured with an accuracy of 0.5° and checked against the Brillouin shifts of the already mentioned fused silica sample, while an f-number of 1:20 or a properly reduced angular aperture was adopted in order to neglect the line broadening due to the finite collection angle.

The sample, 99% purity research grade glycerol purchased from Sigma Aldrich, was embedded into a cylindrical 20 mm external diameter 18 mm internal diameter quartz cell thermoregulated by external fluid circulation. Temperature stability was controlled by means of a Pt500 sensor and found to be better than ±0.5 K during the integration time of each spectrum of typically 30 min.

In figure 1 we report a selection of BLS and BUVS spectra, $I(q, \omega)$, collected at constant temperature in the V–U geometry (vertical polarization of incident beam and unpolarized scattered intensity). The spectra are reported as obtained after normalization for the second spectral moment $\int_{-\infty}^{\infty} \omega^2 I(q, \omega)\, \mathrm{d}\omega$.

The inelastic peak position is shown by vertical arrows and the two limiting linear dispersions are also reported as straight dotted lines for comparison. The low Q limit value was derived from US measurements [13], while the opposite limiting value is obtained from our IXS data and seems fully consistent with what was reported in [2]. The remarkable dispersive effect induced by the active relaxation process can be readily noticed looking at the more-than-linear q dependence of the peak position of the spectra.

Similar measurements of the evolution of $S(q, \omega)$ with q were repeated at the following temperatures: 297, 308, 318, 328 and 338 K. The effective values of $q = (4\pi/\lambda)n \sin(\theta/2)$ were evaluated through appropriate estimations of the refractive index $n = n(\lambda, T)$. The temperature dependence was estimated using the Clausius–Mossotti law, where the mass density was retrieved from literature data [20]. The λ dependence of n was, instead, estimated by extrapolating the available literature measurements [21].

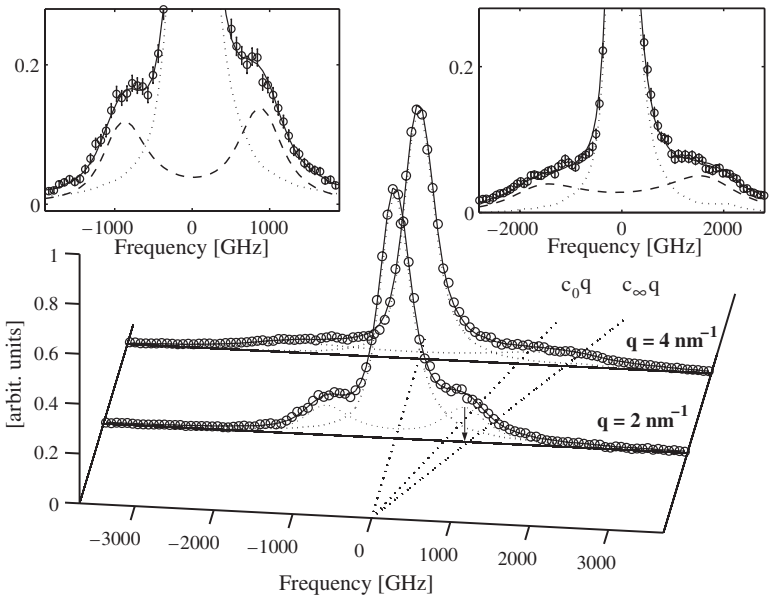

Figure 2. IXS spectra of glycerol collected at $T = 298$ K and corresponding to $q = 2$ and 4 nm^{-1}. The data (○) are compared with the best fit curves of equation (3) (solid line). The DHO (dashed line) and elastic (dotted line) contributions obtained with the fit procedure by using the model in the equation (3) are also shown as dotted lines. The same lineshapes are shown in the two insets as they appear in a restricted quasi-elastic frequency window where inelastic shoulders are clearly discernible.

2.2. IXS measurements

The spectrometer used, at present working at one of the high-resolution IXS beamlines of the ESRF, ID28, consists of a back-scattering Si monochromator crystals and five independent Si analysers, mounted on the tip of a 7 m long arm and separated by an angular offset, so as to allow the simultaneous collection of spectra at five different exchanged momenta. The scattering angle can be chosen by rotating the arm in the horizontal plane to select the desired q value; the q resolution was set to ± 0.2 nm^{-1}.

The working principle of the spectrometer, described in further detail elsewhere [22], is based on high-order reflections from perfect silicon single crystals in extreme back-scattering geometry. The source is an undulator tuned to exploit the Si(11, 11, 11) reflection from the main monochromator, corresponding to a beam energy of 21.747 keV.

The instrumental resolution function was measured by collecting the spectral density of a Plexiglas sample around its first diffraction peak ($q = 10$ nm^{-1}); the corresponding spectrum mainly consists of a featureless sharp peak having a full width at half maximum of 1.5 ± 0.1 meV for each of the five analysers. The spectral intensity coming from the cell windows was measured and found to yield a negligible contribution to the spectrum.

In figure 2 we report the measured IXS spectra collected at $q = 2$ and 4 nm^{-1}, respectively, for the four temperatures 298, 308, 318 and 338 K. The persistence of clear inelastic shoulders can be readily appreciated, the position of which is much higher than expected in the viscous limit and rather closer to the infinite frequency (elastic) one. The same lineshapes are reported in the two insets to put emphasis on the spectral behaviour in the quasi-elastic region.

3. Theoretical background

An inelastic scattering experiment allows a direct measurement of the dynamic structure factor, $S(q, \omega)$:

$$S(q, \omega) = \frac{S(q)}{2\pi} \int_{-\infty}^{\infty} \mathrm{d}t \, \mathrm{e}^{-\mathrm{i}\omega t} \Phi_q(t), \tag{1}$$

where we have introduced the intermediate scattering function as:

$$\Phi_q(t) = \frac{\langle \delta\rho_q^*(0)\delta\rho_q(t)\rangle}{\langle \delta\rho_q^*(0)\delta\rho_q(0)\rangle}. \tag{2}$$

Here $\delta\rho_q(t)$ is the q component of the density fluctuation, $\delta\rho(\mathbf{r}, t)$, and $S(q)$ is the static structure factor. The dynamic structure factor determines the IXS cross section, and the leading part of the BLS and BUVS ones. However, our inelastic light and ultraviolet spectra also contain, beside the two Brillouin peaks, two other contributions. One, belonging to the isotropic part of the spectrum, is the well-known Mountain peak that in molecular liquids arises from the coupling of acoustic modes with both the α process and with molecular internal degrees of freedom (see [23, 8]); the other is the depolarized component arising from anisotropic fluctuations. The latter has been found to yield a negligible influence on both the widths and positions of the inelastic peaks, the two parameters of interest in this study. Therefore these contributions will be simply discarded in the following discussion.

In the hydrodynamic, low-q, limit, the Navier–Stokes theory of hydrodynamics provides an accurate description of the dynamic structure factor. Within the further hypothesis of slowly relaxing diffusive thermal motion, rather appropriate for liquid glycerol, the Navier–Stokes description leads to:

$$\frac{S(q, \omega)}{S(q)} \simeq \frac{\gamma - 1}{\gamma}\delta(\omega) + \frac{1}{\gamma}\frac{1}{\pi}\frac{\Omega^2(q)\Gamma(q)}{(\omega^2 - \Omega^2(q))^2 + \Gamma(q)^2\omega^2}. \tag{3}$$

Here $\Omega(q)$ and $\Gamma(q)$ are the position and the width of the Brillouin peaks, respectively, while $\gamma = c_p/c_v$ represents the ratio of specific heats at constant pressure and constant volume. This hydrodynamic expression of the dynamic structure factor provides an accurate description of the spectral lineshape as far as $D_\mathrm{t}q^2 \ll \Omega(q)$ and $\Gamma(q) \ll \Omega(q)$, where D_t is the thermal diffusivity of the liquid. Hypersonic parameters can be easily related to the adiabatic sound velocity, c_s, and the longitudinal kinematic viscosity, D_ν, through

$$\Omega(q) = c_\mathrm{s}q \tag{4}$$

$$\Gamma(q) = D_\nu q^2 = \frac{\eta_\mathrm{B} + \frac{4}{3}\eta_S}{\rho}q^2 \tag{5}$$

where ρ is the mass density of the fluid and η_B and η_S are the bulk and shear components, respectively, of the viscosity coefficient. Therefore the first hydrodynamic condition ($D_\mathrm{t}q^2 \ll \Omega(q)$) means that thermal motions are much slower than the typical period of the acoustic wave, which thus propagates without thermal exchanges with the local environment. In this limit of low thermal conductivity, thermal fluctuations contribute only to the low-frequency region of the spectrum, giving rise to the Rayleigh peak centred at frequency zero and with a linewidth well above our instrumental resolution. The second condition ($D_\nu q^2 \ll c_\mathrm{s}q$) means that acoustic waves have a lifetime much longer than their period. Both these condition are well known to be fulfilled by liquid glycerol at higher than GHz frequencies and q higher than 0.01 nm^{-1}.

In equation (3) the elastic line is accounted for by $\delta(\omega)$ and the Brillouin doublet is approximated by a damped harmonic oscillator profile. Unfortunately the Brillouin

spectroscopic technique employed does not allow the separation of the two (shear and bulk) component of the viscosity, preventing their characterization in respect of q dependence.

Clearly, equation (3) follows the hydrodynamic approximation for which Ω and Γ only depend on q. When a relaxation is active in the fluid such assumptions break down and frequency dependences becomes important.

Within the generalized hydrodynamics approach the finite-ω extension of the hydrodynamic description can be achieved by keeping the formal structure of equation (3) unchanged yet allowing the involved transport parameters (equations (4) and (5)) to become appropriate functions of frequency. Such frequency dependence reflects the discussed ω transition between viscous (zero frequency) and elastic (infinite frequency) regimes, and, in a spectroscopy experiment, is expected to be described by a non-trivial q dependence.

The various models developed in the attempt to describe such viscoelastic crossover have a merely phenomenological character. One of the most popular stems from the assumptions that the time decay of hypersonic parameters can be well approximated by a stretched exponential of the form $\exp(\frac{-t}{\tau})^{\beta}$. The corresponding ω dependence can be derived from such a distribution through a Laplace transform fairly well approximated by a Cole–Davidson (CD) profile [24], which for the sound velocity prescribes:

$$c_s^2(\omega) = c_\infty^2 - (c_\infty^2 - c_0^2)\,\mathrm{Re}[h(\mathrm{i}\omega)], \tag{6}$$

while for the longitudinal kinematic viscosity

$$D_\nu(\omega) = D_\nu^\infty + (c_\infty^2 - c_0^2)\,\mathrm{Re}\left(\frac{1 - h(\mathrm{i}\omega)}{\mathrm{i}\omega}\right), \tag{7}$$

where

$$h(\mathrm{i}\omega) = \left(\frac{1}{1 + \mathrm{i}\omega\tau}\right)^{\beta}.$$

Here c_0 (c_∞) and D_ν^0 (D_ν^∞), represent the viscous (elastic) limit of the sound velocity (longitudinal kinematic viscosity), while τ and $\beta \leqslant 1$ are the relaxation time and the stretching parameter.

4. Data analysis

The spectra have been fitted by the hydrodynamic model of equation (3) convoluted with the instrumental resolution, $R(\omega)$. The best fit to the data is obtained through a χ^2 minimization of the following fitting function:

$$f(q, \omega) = A \cdot R(\omega) \otimes S(q, \omega) + B \tag{8}$$

where the parameters A and B account for an overall intensity amplitude and a flat background respectively. For all (low and high q) spectra we have used the same model expressed by equation (3) where $\Gamma(q)$ and $\Omega(q)$ have been assumed as totally free lineshape parameters. However, some precautions were adopted while performing lineshape analysis, according to the specific dynamic range involved:

Low-q spectra

It is worthwhile remarking that equation (3) provides a poor description of the low-q lineshape, mainly in the region of spectral wings and for frequencies slightly lower than the inelastic peak positions. This inadequacy clearly emerges even from a first inspection of figure 3, where the spectrum corresponding to $\omega\tau(q, T) \simeq 1$ is shown and compared with the corresponding best fit lineshape. The observed discrepancy strongly suggested ruling out the quasi-elastic region while fitting the spectral lineshapes of BLS and BUVS spectra.

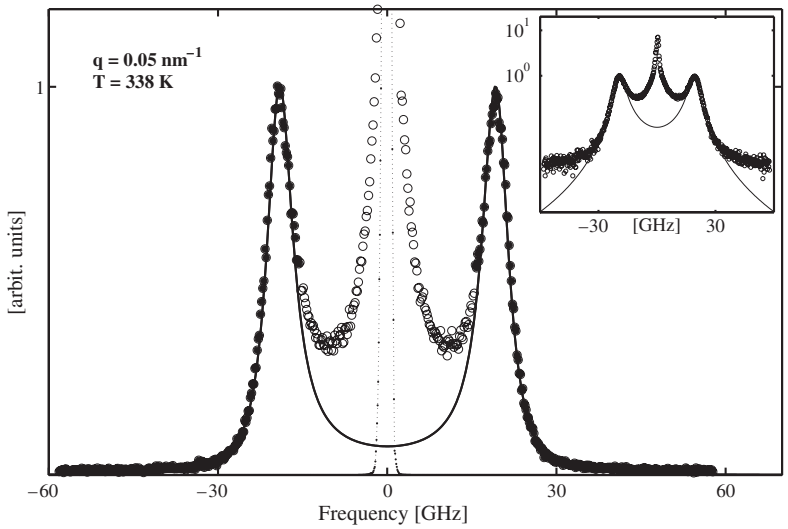

Figure 3. BUVS spectrum of glycerol collected at $T = 338$ K and at $q \simeq 0.05$ nm^{-1}. The spectrum is compared with both the experimental resolution function (:) and the best fit lineshape (solid line). The lineshapes have been fitted in a limited region (●) ruling out the low-energy portion (○). The datum is also plotted in the inset in logarithmic scale to emphasize the mismatch between V–U spectra and the model used in both spectral wings and quasi-elastic regions.

High-q spectra

A rigorous description of high-q (high frequency) IXS spectra requires a modification of equation (3) which accounts for the quantum character of the lineshape. The latter, owing to detailed balance, gives rise to a clear asymmetry of the spectral density, which has been simply retrieved by adding a prefactor to equation (3) as follows:

$$S_{\mathrm{IXS}}(q,\omega) = \frac{\hbar\omega}{k_{\mathrm{B}}T}[n(\omega)+1]S(q,\omega), \tag{9}$$

where $n(\omega)$ is the usual Bose–Einstein population factor. Best fit lineshapes of IXS spectra have been reported in figure 2 together with the separate inelastic component.

5. Discussion

As recalled in the previous section, the DHO model, despite poorly describing the detail of the spectral lineshape, allows a reliable evaluation of both the position and width of the Brillouin doublet. A straightforward evaluation of the sound velocity and the kinematic viscosity can thus be obtained from these quantities through equations (4) and (5) respectively.

As already pointed out, while going from viscous to elastic regimes the energy losses affecting acoustic propagation are considerably reduced. Therefore, we expect to correspondingly observe both a monotonic decrease in longitudinal viscosity and an increase in apparent sound velocity.

Both these expectations are retrieved by the c_{s} and D_ν data reported in figures 4 and 5, respectively. There, experimental data are plotted as a function of the proper frequency $\nu = c_{\mathrm{s}}q/2\pi$ (c_{s} being evaluated from the peak positions). In the same figure, the profile in equation (6) (equation (7)) which best fits c_{s} (D_ν) data is also reported for comparison as a solid line. The best fit curves have been obtained keeping β, D_ν^∞ and τ as free parameters

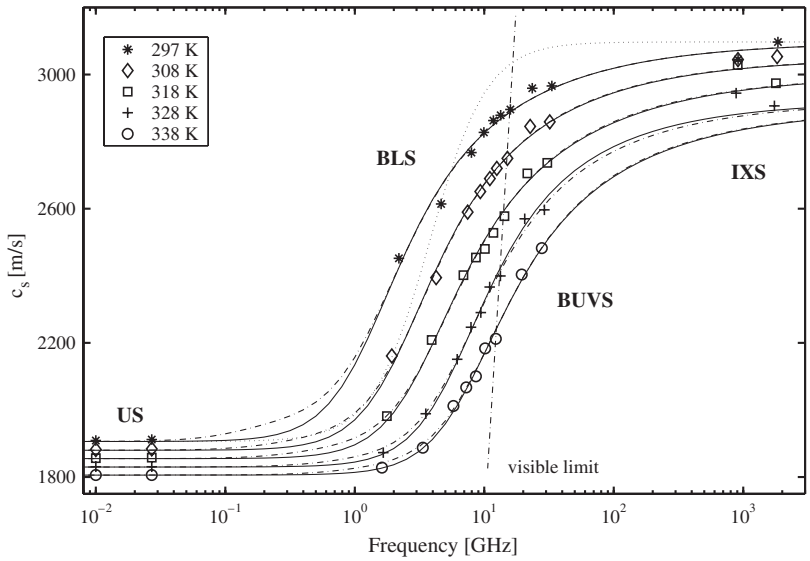

Figure 4. Sound velocity data derived from the best fit parameters of the model in equation (3). Data refer to visible, ultraviolet and IXS Brillouin spectra at the different exchanged wave vectors and at the T indicated in the plot. The low-frequency data [10, 27 MHz] are obtained from ultrasound measurements reported in [13]. Data are compared with Cole–Davidson profiles (solid curves) which best fit experimental data (see equation (6)). A simple viscoelastic distribution (see text) best fitting of the lowest-temperature datum is also reported for comparison (dotted line). Finally dash–dotted lines represent best fit curves achieved with a Cole–Davidson profile plus the additional viscoelastic term (see text).

of the fitting procedure to vary without any constraint. Conversely the parameter c_0 has been fixed to the values derived from US measurements reported in [13] and c_∞ has been fixed to the values evaluated from our highest q (IXS) spectra. As far as US measurements are concerned, D_ν values have been extracted from the α parameter through $\frac{\alpha}{f^2} = \frac{2\pi^2}{c_s^3} D_\nu$, from which, with $\Gamma_{\mathrm{FWHM}} = D_\nu q^2$ and $f = \frac{\omega}{2\pi} = \frac{c_s q}{2\pi}$, it follows that

$$\Gamma_{\mathrm{FWHM}} = c_s \cdot 2\alpha.$$

On rigorous grounds US essentially probes the modulus relaxation time, τ^{US}, while GHz and THz spectroscopies probe the compliance time τ. Therefore to keep consistency with our results US τ^{US} values should be multiplied by c_∞^2/c_0^2.

Comparing the best fits obtained with the CD profile with experimental data, some general features clearly emerge and deserve some comment:

(a) *As far as the sound velocity* data (figure 4) are concerned, we note that:

(i) The inflection point of various constant-T curves is pushed towards higher frequencies while increasing T. This behaviour witnesses the sharp T dependence of the involved relaxation timescale as typical of the glass forming systems and definitely reveals the structural character of the probed relaxation process. A structural origin seems further supported by the results presented in figure 6 where the relaxation timescale is reported in an Arrhenius plot.

(ii) Even if c_0 (c_∞) have been fixed to the lowest (highest) frequency experimental values, the consistency of theoretical profiles with all data reported is still surprising; in fact, the latter are carried out from independent measurements covering disparate frequency windows, which span from the MHz to the THz ranges.

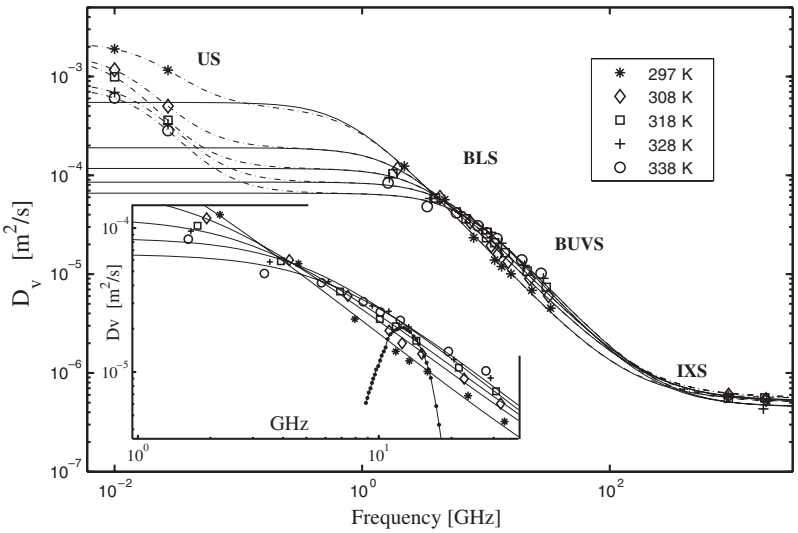

Figure 5. Kinematic longitudinal viscosity derived from best fit parameters of the model in equation (3). Symbols are the same as for figure 4. Data are compared with Cole–Davidson profiles (solid curves) which best fit experimental data (see equation (6)). Dash–dotted lines represent best fit curves achieved with a Cole–Davidson profile plus the additional viscoelastic term (see text). The inset shows the frequency dependence of data around the inflection region. Literature BLS data of [2] are also reported there for comparison (— · —).

(iii) In figure 4 the profile corresponding to the single timescale ansatz ($\beta = 1$) and best fitting of the coldest $c_s(\omega)$ datum is also reported for comparison. The agreement with experiment is rather poor as compared with that of the CD profiles.

(b) *Longitudinal kinematic viscosity* curves reported in figure 5 suggest the following comments:

(i) Even if error bars are not available, the US data of [13] definitely lie above our single-timescale best fit CD curves. However, such US measurements are of appreciable quality, and seem fully consistent with both (zero frequency) calorimetric measurement of [24] and ISTS data of [19]. The consistency of the various low-frequency measurements and the discrepancy with higher-frequency ones ([2] and our result) strongly suggest the occurrence of additional intermediate-frequency relaxation processes probably influencing the bulk component of the viscosity, η_B. They should be active in a dynamic range lying below the sensitivity of the present experiment, in which we mainly probe structural rearrangements involving shear viscosity.

(ii) In the inset we also show BLS measurements of $D_\nu(T)$ achieved at nearly constant q and reported in [2]. The curve reaches a maximum at $T = 353$ K, where the condition $c_s q = 1/\tau_0(T)$ is matched. This allows us to derive $\tau_0(353\ \text{K}) = 11$ ps, in fair agreement with our highest T determination shown in figure 6. Indeed the consistency between a T-dependent determination [2] and an ω (time)-dependent one (this work) provides a further evidence of the so-called time–temperature superposition principle.

Once the occurrence of an additional slow relaxation has been inferred from $D_\nu(\omega)$ data a further analysis was performed with a slightly complex model accounting for such a process by means of an additional simple relaxation term, SR, ($\beta = 1$). While performing such a SR + CD fit the viscoelastic timescale (τ_1) and the intermediate elastic velocity ($\bar{c}$) were taken

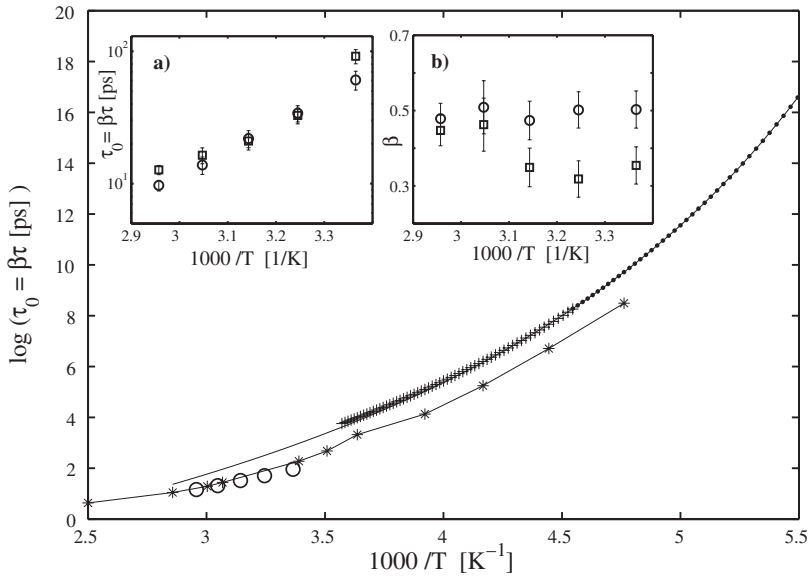

Figure 6. Arrhenius plot of the mean relaxation time $\tau_0 = \tau\beta$ obtained from the best fit of the sound velocity data of figure 4. We also show literature BLS data from [2] ($\star$), ISTS data from [19] (+), and the specific heat measurements from [17] (a) ($\bullet$). Moreover the Vogel–Tamman–Fulker curve best fitting data of [19] and [17] is also reported for comparison (solid line). In the inset the stretching parameter β is reported. Open circles represent the best fit parameters of c_s data, while open squares are the best fit values determined with D_ν measurements.

as additional free parameters. The introduction of τ_1 and $\bar{c}$ define the VE dispersive step of the sound velocity.

The best fit values of $\bar{c}$ differ from c_0 by only a few per cent; consequently, the SR dispersive step of the sound velocity is rather weak ($\propto[\bar{c} - c_0]$) as compared with that of the kinematic viscosity ($\propto[\bar{c}^2 - c_0^2]$). This has prevented us from achieving a reliable determination of τ_1 and $\bar{c}$ from the $c_s(\omega)$ data. Since D_ν is more sensitive to the presence of the SR term, only $D_\nu(\omega)$ measurements were used to determine τ_1 and $\bar{c}$. Then the resulting best fit values were inserted in the model SR + CD profiles of the sound velocity obtaining the dashed curves reported in in figure 4.

The effects of the additive SR term clearly emerge when comparing solid (CD) and dot–dashed (CD + SR) curves reported in figures 4 and 5: the presence of the SR term noticeably improves the agreement with US data (figure 5) leaving the sound velocity profiles almost unchanged (figure 4).

As a matter of fact the τ_1 values have been found to be higher than $\beta\tau$ by almost an order of magnitude, thus falling definitely over the sensitivity of the present experiment.

The values of the mean relaxation time $\tau_0 = \beta\tau$ and the stretching parameter β, derived from best fit with the CD profiles of equations (6) and (7), are shown in figure 6 in an Arrhenius plot. In the same figure the literature BLS [2], impulsive stimulated thermal scattering ISTS [19] and specific heat measurements [17] are also reported for comparison.

We recall that for intermediate glass formers, such as glycerol, the T dependence of $\langle\tau\rangle$ is expected to parallel that of the shear viscosity, i.e. to follow the VTF law, $g(T) = e^{(\frac{w}{T-T_0})}$, and that deviations from such behaviour are expected only near the glass transition temperature where relaxation time is essentially a non-equilibrium parameter. Figure 6 also shows the VTF

best fit of data from [19] extrapolated to our temperature for a direct comparison, while in the two insets we show, in a more restricted T range, the τ_0 and β parameters. There the open circles represents the best fit values of c_s data, while the open squares are the best fit values obtained with D_ν measurements.

The data shown in figure 6 suggest the following remarks:

(i) The T dependence of our τ_0 measurements is compatible with a VTF law, as expected for fragile glass formers. However, the involved parameters w and T_0 can hardly be evaluated because of both the narrow range and the high temperature values probed.

(ii) In the overlapping T range we find good consistency between the present τ_0 values and the literature BLS ones.

(iii) The τ_0 measurements achieved by BLS and IXS, in the GHz and THz windows, respectively, are slightly lower than the calorimetric and the ISTS determinations. Once again, this suggests the occurrence of a slow relaxation involving the bulk component of the viscosity and belonging to a time domain lying above the sensitivity of BLS and IXS.

(iv) The τ_0 values obtained by fitting $c_s(\omega)$ and $D_\nu(\omega)$ (open circles and squares respectively, in inset (a)) are fairly consistent with each other. This highlights the occurrence of a similar time decay mechanism of the sound velocity and of the longitudinal viscosity.

(v) The β values determined by the best fit of $c_s(\omega)$ (open circles in inset (b)) are almost insensitive to temperature changes remaining nearly constant at a value of $\simeq 0.5$, in fair agreement with previous BLS measurements.

(vi) Conversely, the β values obtained as best fit parameters of $D_\nu(\omega)$ (open squares in inset (b)) slightly decrease with lowering T, indicating a corresponding broadening of the CD distribution. In view of the mentioned time–temperature superposition principle it seems natural to associate this low T trend at low frequency of those slow relaxation processes already thoroughly discussed.

6. Conclusion

In conclusion, we have carried out a joint experimental study of the dynamics of high-temperature liquid glycerol performed by complementary spectroscopic techniques, such as Brillouin visible, ultraviolet and x-ray scattering. The spectra were collected as a function of both momentum transfer and temperature. To our knowledge, this represents the first attempt to map the quite large frequency domain extending from the GHz to the THz and ideally bridging, at lower frequencies, the gap existing with ultrasound techniques.

A best fit lineshape analysis with a simple hydrodynamic model has enabled us to extract the values of frequency-dependent transport parameters such as the sound velocity and the longitudinal kinematic viscosity. As a result we observe their frequency dependence to be quite closely approached by a Cole–Davidson frequency distribution. Despite the large jump in the frequency windows explored the presented data are self-consistent and show fair agreement with MHz measurements. Moreover, once compared with T-dependent BLS results from the literature, they provide strict evidence of the so called time–temperature superposition principle.

Some discrepancies are instead observed with US measurements of kinematic viscosity, which are ascribed to slow rearrangements involving the bulk component of viscosity and occurring in a frequency domain lying below the GHz threshold.

Finally, the mean relaxation time and the stretching parameter have been extracted through best fit of both sound velocity and kinematic viscosity data. The observed T dependence of

relaxation timescales seems compatible with a VTF law, as expected for glass formers, though absolute values are, owing the reason recalled above, a bit lower than lower-frequency ones.

Finally, we recall that the model used, despite providing a reliable determination of both inelastic peak positions and widths, poorly describes the spectral density at relatively low frequencies. This argument motivated us to improve the spectral analysis using a more refined and physically informative theoretical model based on the Mori–Zwanzig formalism of the memory function [12]. The use of this last refined model allows us to determine, from the spectral lineshape, the viscous and elastic limiting values of relevant transport parameters as well as the relaxation timescale involved. Such a study is in progress and will be the subject of a forthcoming publication.

Acknowledgments

The authors wish to acknowledge Professor M Nardone and Dr P Benassi for useful discussions and support during the experiment and Dr S Falconi for valuable help during the preparation of the manuscript.

References

[1] Slie W M, Donfor A R and Litovitz T A 1966 *J. Chem. Phys.* **44** 3712
[2] Comez L, Fioretto D, Scarponi F and Monaco G 2003 *J. Chem. Phys.* **119** 6032
[3] Scopigno T, Balucani U, Ruocco G and Sette F 2001 *Phys. Rev.* E **63** 011210
Scopigno T, Di Leonardo R, Ruocco G, Baron A Q R, Tsutsui S, Bossard F and Yannopoulos S N 2004 *Phys. Rev. Lett.* **92** 025503
[4] Cunsolo A and Nardone M 1996 *J. Chem. Phys.* **105** 3911
[5] Cunsolo A, Ruocco G, Sette F, Masciovecchio C, Mermet A, Monaco G, Sampoli M and Verbeni R 1999 *Phys. Rev. Lett.* **82** 775
Monaco G, Cunsolo A, Ruocco G and Sette F 1999 *Phys. Rev.* E **60** 5505
[6] Maisano G, Migliardo P, Aliotta F, Vasi C and Wanderlingh F 1984 *Phys. Rev. Lett.* **52** 1025
Maisano G, Majolino D, Mallamace F, Migliardo P, Aliotta F, Vasi C and Wanderlingh F 1986 *Mol. Phys.* **57** 1083
[7] Levesque D, Verlet L and Kürkijarvi J 1973 *Phys. Rev.* A **7** 1690
Ruocco G, Sette F, Di Leonardo R, Monaco G, Sampoli M, Scopigno T, Viliani G, Wojcik M and Clementi E 1986 *J. Chem. Phys.* **85** 6085
[8] Boon J P and Yip S 1991 *Molecular Hydrodynamics* (New York: Dover)
Balucani U and Zoppi M 1994 *Dynamics of the Liquid State* (Oxford: Clarendon)
Herzfeld K F and Litovitz T A 1965 *Absorption and Dispersion of Ultrasonic Waves* (London: Academic)
[9] Goetze W and Sjoegren L 1992 *Rep. Prog. Phys.* **55** 241
[10] Schneider U, Lunkenheimer P, Brand R and Loidl A 1998 *J. Non-Cryst. Solids* **235** 173
[11] Angell C A 1984 *Relaxation in Complex Systems* ed K L Ngai and G B Wright (Washington, DC: NRL)
[12] Zwanzig R 1961 *Lectures in Theoretical Physics* vol 3, ed W Brittin (New York: Wiley–Interscience) pp 106–41
Mori H 1965 *Prog. Theor. Phys.* **33** 423
[13] Jeong Y H, Nagel S R and Battacharya S 1986 *Phys. Rev.* A **34** 602
Jeong Y H 1987 *Phys. Rev.* A **36** 766
[14] Sette F, Krisch M, Masciovecchio C, Ruocco G and Monaco G 1998 *Science* **280** 1550
[15] Wuttke J, Hernandez J, Li G, Coddens G, Cummins H Z, Fujara F, Petry W and Sillescu H 1994 *Phys. Rev. Lett.* **72** 3052
[16] Benassi P, Eramo R, Giugni A, Nardone M and Sampoli M 2005 *Rev. Sci. Instrum.* **76** 013904
[17] Birge N O and Nagel S R 1985 *Phys. Rev. Lett.* **54** 2674
Rajeswari M and Raychaudhuri A K 1993 *Phys. Rev.* B **47** 3036
[18] Shonhals A, Kremer F, Hofmann A, Fischer E W and Schlosser E 1993 *Phys. Rev. Lett.* **70** 3459
[19] Paolucci D M and Nelson K A 2000 *J. Chem. Phys.* **112** 6725
[20] McDuffie G E, Forbes J W, Madigosky W M and Von Bretzel J J 1969 *J. Chem. Eng. Data* **14** 176
[21] Reheims J, Kōser J and Wriedt T 1997 *Meas. Sci. Technol.* **8** 601–5

Landolt-Bőrnstein 1996 *Group III: Condensed Matter* (*Optical Constants, New Series* vol A) vol 38 *Refractive Indices of Inorganic, Organometallic and Organometallic Liquids and Binary Liquid Mixtures* ed W Marterseen (Berlin: Springer)

[22] Masciovecchio C, Bergmann U, Krisch M, Ruocco G, Sette F and Verbeni R 1996 *Nucl. Instrum. Methods* B **117** 339

[23] Mountain R D 1966 *Rev. Mod. Phys.* **38** 205
Mountain R D 1966 *J. Res. Natl Bur. Stand.* A **70** 207

[24] Cole K S and Cole R H 1941 *J. Chem. Phys.* **9** 341
Cole R H and Davidson D W 1952 *J. Chem. Phys.* **20** 1386